

# Electrodeposition of Thermoelectric Films Co<sub>x</sub>Ni<sub>(1-x)</sub>Sb<sub>3</sub> and Co-Sb<sub>x</sub>Te<sub>(1-x)</sub> in Citrate Solutions

Ruxandra Vidu, Maria Perez-Page, Dat V. Quach, Pieter Stroeve

Department of Chemical Engineering and Material Science  
University of California, Davis, 95616, United States  
\*rvidu@ucdavis.edu

**Abstract:** Skutterudite compounds were studied as new potential candidates for thermoelectric applications. CoSb<sub>3</sub> showed good electrical properties and doping this material with nickel and tellurium would improve the thermoelectric properties. In this work the mechanisms for the electrodeposition of cobalt, nickel, antimony and tellurium in citrate solutions on a nanostructured gold template was studied. Comprehensive deposition-stripping experiments have been performed in order to understand the mechanism of the co-deposition of cobalt and antimony, as well as of the Ni and Te dopants. The results showed that there were two mechanisms operating in this system, i.e. the deposition of Co and Ni is controlled by the electrochemical reaction at the Au electrode, while Sb and Te depositions are controlled by diffusion. Although the experiments were performed in an electrolyte that contained citrates to form Sb and Te complexes and to increase the solubility of Sb<sub>2</sub>O<sub>3</sub> and TeO<sub>2</sub>, the deposition of Sb and Te is still controlled by diffusion due to their low solubility.

## Introduction

Driven by the high price of crude oil and global efforts to reduce carbon dioxide emission, the research on alternative and renewable energy sources has been shown a great development. In addition to their applications in electronic refrigeration for the ever smaller computer chips and circuit boards, thermoelectric materials can be used to extract energy from waste heat and convert it to electricity. Thermoelectric materials directly convert heat to electricity based on the Seebeck effect [1].

Cobalt triantimonide, CoSb<sub>3</sub>, shows promising thermoelectric properties at intermediate temperatures (400 - 700 °C), with most research focusing on reducing lattice thermal conductivity by introducing large heavy atoms into the skutterudite structures. The efficiency of a thermoelectric material is determined by its dimensionless thermoelectric figure of

merit, ZT, that can be expressed by eq. 1 [1, 2]:

$$ZT = \frac{S^2 \cdot \sigma \cdot T}{\kappa} \quad (1)$$

where,  $S$  is the Seebeck coefficient,  $\sigma$  is the electrical conductivity,  $\kappa$  is the thermal conductivity and  $T$  is the absolute temperature. Thermal conductivity property is a result of both electronic ( $\lambda_E$ ) and lattice conductivity ( $\lambda_L$ ) contributions. A good thermoelectric material should possess a large power factor ( $S^2 \sigma$ ) and a low thermal conductivity, so that the temperature difference between the heat source and the cold side is maintained constant.

Skutterudites, especially of n-type conductivity, are of special interest due to their excellent electrical transport properties and large Seebeck coefficient. Unfortunately, the thermal conductivities of the binary skutterudites are too large for thermoelectric applications. In order to optimize conflicting electric and thermal

properties such as those required by thermoelectric materials, a variety of compositional, structural and dimensional modifications are required [3].

The effects of doping with various donor impurities on the thermoelectric properties of polycrystalline  $\text{CoSb}_3$  have been extensively studied [4]. The analysis of the transport properties suggests that the electronic properties depend strongly on both the donor impurities (either fillers or dopants) and the carrier concentration, which control not only the electronic transport properties but also the scattering mechanisms of phonons in heavily doped n-type  $\text{CoSb}_3$ . The substitution of Co or Sb in  $\text{CoSb}_3$  with different dopants can influence the electronic structure and the electrical properties, in particular by changing the carrier masses. Furthermore, doping affects the lattice thermal conductivity due to phonon scattering on impurities. Dopants such as Ni, to replace Co, and Te, to replace Sb, can be used to further optimize the electrical conductivity and effectively scatter phonon [2, 4, 5].

### Experimental procedure

Electrochemical experiments were performed in a conventional three-electrode set up. The counter electrode was an Au wire and the reference electrode was a Ag/AgCl electrode (3M NaCl). All potentials are relative to Ag/AgCl (+0.210V vs standard hydrogen electrode). A computer-controlled potentiostatic (model AFCBP1, Pine Instrument Company) was used for cyclic voltammetry, deposition-stripping experiments and potentiostatic cathodic electrodeposition. The Aftermath software (National Instruments, TX, USA) was used to control the potentiostat.

Gold sputtered polycarbonate track-etched (PCTE) membranes (GE Water & Process Technologies, PA, USA) were used as substrates for deposition. The PCTE template is 10  $\mu\text{m}$  thick, and the pore diameters are approximately 400 nm

in average. One side of the PCTE membranes was sputtered with Au. The area occupied by the pores for the 400 nm membranes was 12.57%.

The Au-coated, PCTE template was then placed on a copper tape and mounted in between two plastic masking tapes, one of them with a circular cut-out, exposing the Au coated side of the PCTE membrane. The circular cut-out had an area of 0.3846  $\text{cm}^2$ . Figure 1 shows the schematic sample setup configuration of the working electrode.

The electrochemistry experiments were performed in aqueous electrolyte solutions containing the chemicals of interest, i.e.  $\text{Sb}_2\text{O}_3$  (99.99%),  $\text{CoSO}_4 \cdot 7\text{H}_2\text{O}$  (>99%),  $\text{C}_6\text{H}_7\text{KO}_7$  (potassium citrate monobasic) (>99.5),  $\text{C}_6\text{H}_8\text{O}_7$  (citric acid) (>99.5%) and/or  $\text{TeO}_2$  (99.995%). All the chemicals were purchased from Sigma-Aldrich. Various aqueous solution were prepared with different concentrations as shown in Table 1

**Table 1:** Composition of different citrate solutions

Solution	Description
(1)	0.125 M $\text{C}_6\text{H}_7\text{KO}_7$ + 0.196 M $\text{C}_6\text{H}_8\text{O}_7$ + 0.003 M $\text{Sb}_2\text{O}_3$
(2)	0.125 M $\text{C}_6\text{H}_7\text{KO}_7$ + 0.196 M $\text{C}_6\text{H}_8\text{O}_7$ + 0.172 M $\text{CoSO}_4$
(3)	0.125 M $\text{C}_6\text{H}_7\text{KO}_7$ + 0.196 M $\text{C}_6\text{H}_8\text{O}_7$ + 0.001 M $\text{TeO}_2$
(4)	0.125 M $\text{C}_6\text{H}_7\text{KO}_7$ + 0.196 M $\text{C}_6\text{H}_8\text{O}_7$ + 0.172 M $\text{NiSO}_4$
(5)	0.125 M $\text{C}_6\text{H}_7\text{KO}_7$ + 0.196 M $\text{C}_6\text{H}_8\text{O}_7$ + 0.003 M $\text{Sb}_2\text{O}_3$ + 0.172 M $\text{CoSO}_4$
(6)	0.125 M $\text{C}_6\text{H}_7\text{KO}_7$ + 0.196 M $\text{C}_6\text{H}_8\text{O}_7$ + 0.003 M $\text{Sb}_2\text{O}_3$ + 0.170 M $\text{CoSO}_4$ + 0.002 M $\text{NiSO}_4$
(7)	0.125 M $\text{C}_6\text{H}_7\text{KO}_7$ + 0.196 M $\text{C}_6\text{H}_8\text{O}_7$ + 2.97 mM $\text{Sb}_2\text{O}_3$ + 0.172 M $\text{CoSO}_4$ + 0.03 mM $\text{TeO}_2$

Before electrodeposition experiments, an electrochemical treatment of the Au surface was performed to clean the surface and to ensure reproducible results during the electrochemical studies [6-10]. This treatment consists of cleaning the surface by cycling the potential between 0 to 1.5 V for 20 times followed by an electrochemical annealing for 20 min at 0.9

V. The electrochemical treatment is carried out in 50 mM H<sub>2</sub>SO<sub>4</sub> aqueous solution at room temperature.

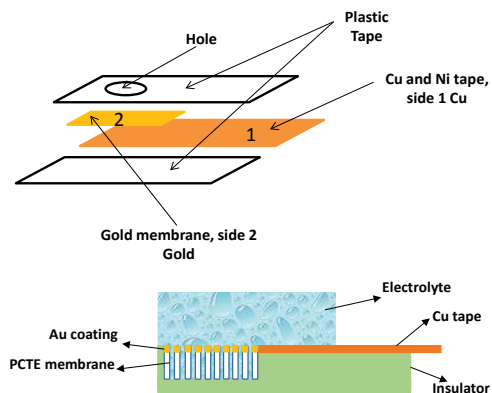


**Figure 1:** Schematic 3D (top) and cross section (bottom) of the set up and working electrode.

Deposition-stripping experiments were performed for each element of interest in its own solution to determine their deposition rates. Deposition was carried out at different potentials between -0.2 and -1.2 V for 5 or 10 min followed by stripping. Solutions were magnetically stirred during deposition at a rate of 500 rpm.

## Results and Discussion

### Cyclic Voltammetry

In order to better understand the electrochemical co-deposition and doping, cyclic voltammetry was recorded for Au in Co-Sb solutions containing nickel and tellurium, and compared to those obtained in Co-Ni-Sb solution. Figure 2 shows the cyclic voltammograms of Au in solution 6 (Co, Ni and Sb) and 7 (Co, Sb and Te), and compared to solution 5 that contains only Co and Sb. Cyclic voltammograms of Au in a given solution were recorded at a sweep rate of 5 mV/s from -1.2 V to 0.5 V for solution 6 and from -1.2 V to 0.7 V for solution 7.

Cyclic voltammograms of Au in Co-Sb and (Co, Ni)-Sb show two oxidation peaks

and no clear reduction peak. Electrochemical deposition of Co and Sb from their solutions was already published by our group [10, 11]. Hydrogen evolution is significant for this system and may overlap with the deposition peak(s). Adding Ni ions in the electrolyte does not visibly affect the CV. Ni and Co form solid solutions over the entire concentration range and this may be the reason why the two CVs are similar. Unlike Ni, the addition of Te ions drastically changes the CV, i.e. additional deposition and stripping peaks appear. The potential range for CV in Te-containing Co-Sb solution was extended in the positive direction from 0.5 to 0.7 V, to allow for the deposit to be removed from the surface during stripping. As Figure 2 shows for solution 7, stripping currents are much larger compared to solution 5 and shift to more positive values, suggesting a more complex deposition process in the presence of Te ions. Also, by comparison, Te has a significant impact on the deposition of Co-Sb compared to Ni, since Te deposits first, before Sb [9, 12, 13].

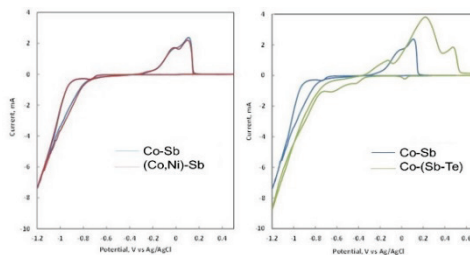


**Figure 2:** Cyclic voltammetry of Au in Co-Sb, Co-Ni-Sb and Co-Sb-Te solutions at 5 mV/s.

### Deposition-stripping experiments

In order to assess the deposition rate of each element of interest, i.e. Co, Sb, Ni, and Te in their individual solutions, a novel deposition-stripping experiment has been designed and performed. Figure 3 shows a typical plot of the current recorded during the deposition performed at a given potential within the potential range from -

0.55 V to -1.2 V, and the current recorded during the stripping performed at 0.4 V i.e. the potential where stripping of the entire deposit is concluded [11]. In Figure 3, a negative current indicates a reduction (deposition) process at the working electrode while a positive value means oxidation (stripping). Electrochemical deposition starts with a very short period of nucleation followed by growth, as indicated by a sharp increase in current followed by stabilization. At the negative end of the potential scanned, the total current is a combination of charge transfer due to both hydrogen evolution and material deposition. During stripping, the current increases rapidly until it reaches a maximum value, as the material that was deposited is removed, and then the current drops to zero.

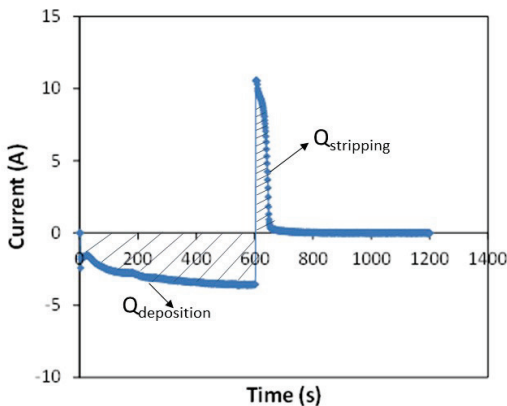


**Figure 3:** Typical plot of current during deposition-stripping experiment at a certain potential

In the absence of hydrogen evolution, the two charges associated with deposition and stripping should be equal. Obviously,  $Q_{\text{deposition}} > Q_{\text{stripping}}$  due to the hydrogen co-deposition with each metal. In any occurrence, the total charge associated with stripping should reflect the amount of metal deposited since hydrogen would actually evolve and not strip. Therefore, the area under the I-t stripping curve ( $Q_{\text{stripping}}$ )

corresponds to the total charge transferred during metal deposition. Using Faraday's Law (eq. 3), the amount of the material removed during stripping can be obtained as follows:

$$m = \frac{Q \cdot M}{F \cdot z} \quad (3)$$

where  $m$  is the mass of the material removed during stripping,  $M$  is its molecular weight,  $F$  is the Faraday's constant (96,485 C/mol) and  $z$  is the valence, which in this case is  $z = 2$  for Co and Ni, 3 for Sb and 4 for Te. Since the amount of the material removed during stripping is equal to the amount of solid materials deposited, the average amount of solid material can be calculated as follows:

$$Q = i \cdot t \quad (4)$$

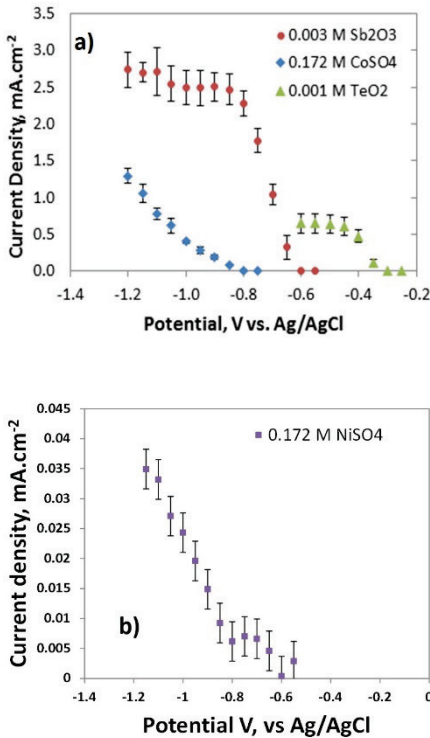
where  $i$  is the current density ( $\text{mA}/\text{cm}^2$ ) and  $t$  is the time (s).

Figure 4 shows the current density due to the deposition of Co, Ni, Sb and Te in their respective citrate solutions, i.e. solution 1, 2, 3 and 4. The deposition of Te does not start until the potential is more negative than -0.3 V. Te deposition rate increases quickly as the potential reaches about -0.45 V, and then remains constant. Results show that when Te was deposited at a potential more negative than -0.6 V, the Te film could not be completely stripped off even when the stripping potential was increased from +0.5 to +0.7 V and held for a more than 10 minutes. Since the stripping data directly affects the calculation of current density during deposition, only results from -0.2 to -0.6 V are shown for Te in Figure 4.a.

For Sb, the deposition starts around -0.65 V and increases quickly as the deposition potential reached -0.8 V. For potentials more negative than -0.8 V, the current density for Sb did not change much and the current stabilized around  $2.58 \text{ mA}/\text{cm}^2$ .

The deposition of Co in a citrate solution containing 0.172 M  $\text{CoSO}_4$  started around -0.85 V. The deposition current

steadily increases as the deposition potential becomes more negative. Same results were observed for Ni, Figure 4.b. The electro-deposition of Ni starts at potentials more positive than Co but more negative than Sb or Te. The main difference between Ni and the other elements is that the current density is much smaller than the current density obtained for Co, at the same concentration of the electrolyte. Because the current densities for Ni deposition are much lower compared to Co, Sb or Te, the results for Ni are shown in a separate chart (Fig.4.b).



**Figure 4:** Deposition rates of Co, Sb, Te, a) and Ni b) in citrate solutions

In the potential range used in this study, the deposition of Co appears to follow the Butler-Volmer equation (eq. 5), and increases with the overpotential increase:

$$i = i_0 \left[ e^{\frac{(1-\beta)\eta F}{RT}} - e^{-\frac{\beta\eta F}{RT}} \right] \quad (5)$$

where  $i$  is the deposition current,  $i_0$  is the equilibrium exchange current,  $\beta$  is the symmetry factor,  $\eta$  is the overpotential,  $F$  is the Faraday's constant,  $R$  is the ideal gas constant and  $T$  is the temperature.

Although the Butler-Volmer equation predicts an increase in the magnitude of the deposition current with overpotential, the reaction rate cannot increase indefinitely with the applied potential because at some point, the diffusion of cations, or complexes containing depositing cations, cannot keep up with the reduction reaction at the electrode. When that instance occurs, the deposition rate is constrained by the diffusion of cations/depositing species and is independent of the deposition potential or overpotential. In this case, the limiting current ( $i_L$ ) is described as :

$$i_L = \frac{z \cdot D \cdot F \cdot C^0}{\delta} \quad (6)$$

where  $z$  is the valence,  $D$  is the diffusion coefficient of the cation,  $\delta$  is diffusion length,  $F$  is the Faraday's constant and  $C^0$  is the concentration of the cation in the electrolyte far away from cathode.

At a given temperature and concentration, the deposition current cannot be greater than the limiting current. This behavior can be seen in Figure 4.a where the current density for Te and Sb remains constant at a large overpotential, which means that Sb and Te deposition are controlled by diffusion.

## Conclusions

Electrochemical studies of Co-Sb doped with tellurium and nickel in citric acid solutions have been performed to better understand the electrochemical doping in these systems.

Electrochemical experiments were carried out to better recognize the deposition of each element of interest in

this system, and the co-deposition of 2 or more elements. The results show that the deposition of Co and Ni is controlled by the electrochemical reaction at the cathode, while Sb and Te depositions are controlled by diffusion. Although the electrolyte contained citrates that form Sb and Te complexes to increase the solubility of  $\text{Sb}_2\text{O}_3$  and  $\text{TeO}_2$ , the deposition of Sb and Te is still controlled by diffusion due to their low solubility. When both Co(II) and Sb(III) are combined in the same citrate solution, their electrochemical behaviors preserve the same characteristics as in single solutions although the relative content of Co is slightly lower. This is probably due to interactions between Co and Sb that give rise to a higher kinetic barrier for the deposition of Co. Deposition of nickel occurs at smaller current densities than other elements and is also controlled by surface reaction.

### References

1. Tritt, T.M. and M.A. Subramanian, *Thermoelectric materials, phenomena, and applications: A bird's eye view*. Mrs Bulletin, 2006. 31(3): p. 188-194.
2. Anno, H., et al., Effects of doping on the transport properties of  $\text{CoSb}_3$ . Journal of Applied Physics, 1999. 86(7): p. 3780-3786.
3. Morelli, D.T., et al., Cerium filling and doping of cobalt triantimonide. Physical Review B, 1997. 56(12): p. 7376-7383.
4. He, Q., et al., Nanostructured Thermoelectric Skutterudite  $\text{Co}_{1-x}\text{Ni}_x\text{Sb}_3$  Alloys. Journal of Nanoscience and Nanotechnology, 2008. 8(8): p. 4003-4006.
5. Wojciechowski, K.T., Effect of tellurium doping on the thermoelectric properties of  $\text{CoSb}_3$ . Materials Research Bulletin, 2002. 37(12): p. 2023-2033.
6. Vidu, R. and S. Hara, In situ EC-AFM observation of Cd electrodeposition on Au(100). Scripta Materialia, 1999. 41(6): p. 617-624.
7. Vidu, R. and S. Hara, Surface alloyed phase formation at Au(100)/ $\text{Cd}^{2+}$  interface during electrodeposition. Electrochemistry, 1999. 67(12): p. 1240-1242.
8. Vidu, R. and S. Hara, In situ electrochemical atomic force microscopy study on Au(100)/Cd interface in sulfuric acid solution. Journal of Vacuum Science & Technology B, 1999. 17(6): p. 2423-2430.
9. Vidu, R., J.R. Ku, and P. Stroeve, Growth of ultrathin films of cadmium telluride and tellurium as studied by electrochemical atomic force microscopy. Journal of Colloid and Interface Science, 2006. 300(1): p. 404-412.
10. Vidu, R., et al., Electrochemical deposition of Co-Sb thin films on nanostructured gold. Journal of Applied Electrochemistry, 2012. 42(5): p. 333-339.
11. Quach, D.V., et al., Electrochemical Deposition of Co-Sb Thin Films and Nanowires. Industrial & Engineering Chemistry Research, 2010. 49(22): p. 11385-11392.
12. Ikemiya, N., et al., Atomic structures and growth morphologies of electro-deposited Te film on Au(100) and Au(111) observed by in situ atomic force microscopy. Surface Science, 1996. 369(1-3): p. 199-208.
13. Ku, J.R., R. Vidu, and P. Stroeve, Mechanism of film growth of tellurium by electrochemical deposition in the presence and absence of cadmium ions. Journal of Physical Chemistry B, 2005. 109(46): p. 21779-21787.